# Oxidative guanine base damage regulates human telomerase activity

Elise Fouquerel[1], Justin Lormand[1,7], Arindam Bose[1,7], Hui-Ting Lee[2], Grace S Kim[3], Jianfeng Li[4], Robert W Sobol[4], Bret D Freudenthal[5], Sua Myong[2,3] & Patricia L Opresko[1,6]

**Changes in telomere length are associated with degenerative diseases and cancer. Oxidative stress and DNA damage have been linked to both positive and negative alterations in telomere length and integrity. Here we examined how the common oxidative lesion 8-oxo-7,8-dihydro-2′-deoxyguanine (8-oxoG) regulates telomere elongation by human telomerase. When 8-oxoG is present in the dNTP pool as 8-oxodGTP, telomerase utilization of the oxidized nucleotide during telomere extension is mutagenic and terminates further elongation. Depletion of MTH1, the enzyme that removes oxidized dNTPs, increases telomere dysfunction and cell death in telomerase-positive cancer cells with shortened telomeres. In contrast, a preexisting 8-oxoG within the telomeric DNA sequence promotes telomerase activity by destabilizing the G-quadruplex DNA structure. We show that the mechanism by which 8-oxoG arises in telomeres, either by insertion of oxidized nucleotides or by direct reaction with free radicals, dictates whether telomerase is inhibited or stimulated and thereby mediates the biological outcome.**

Telomeres cap chromosome ends and are essential for genome stability, cell proliferation and human health. Dysfunctional critically short telomeres trigger cell senescence or apoptosis, which in turn drive aging-related degenerative pathologies and loss of regenerative capacity[1,2]. Telomeres shorten progressively with cell division, owing to the 'end replication problem'. To compensate for this shortening, telomerase lengthens telomeres by adding GGTTAG repeats[3]. In humans, telomeres consist of approximately 1,600 TTAGGG duplex repeats and terminate in a single-strand overhang[4]. Telomerase is expressed in human germ and stem cells, and is upregulated in 90% of cancers, in which it enables continued cell proliferation[4,5]. Thus, telomerase regulation is a critical determinant of degenerative diseases and cancer.

Oxidative stress contributes to the pathogenesis of numerous human diseases including cancer and results from an imbalance between the production of reactive oxygen species (ROS) and cellular antioxidant defenses. The G-rich nature of TTAGGG repeats renders telomeres highly susceptible to oxidative damage, and oxidative stress accelerates telomere shortening[6,7]. ROS are generated as a result of normal oxygen metabolism and pro-oxidant environmental exposures, and are elevated at sites of chronic inflammation[8,9]. Free-radical reactions with DNA generate chemical alterations, including the common lesion 8-oxoG. Oxidative lesions in telomeric DNA are associated with changes in telomere length and integrity[6,7,10].

ROS also react with free-nucleotide pools, and recent studies have underscored the importance of oxidized dNTPs in regulating genome stability and cell survival. Free dNTPs are more susceptible to oxidation than duplex DNA[11], and insertion of oxidized nucleotides into the genome during replication leads to mutations and cell death[12–14]. Nudix hydrolase 1 (NUTD1 or MTH1) converts 8-oxodGTP to 8-oxodGMP, thereby preventing its utilization during DNA synthesis[15]. MTH1 upregulation occurs frequently in various cancers[16,17]. Cancer cell lines are addicted to MTH1, partly because of dysfunctional redox regulation[18,19], and are more sensitive than normal cells to MTH1 inhibitors[14,17]. However, the effects of oxidized dNTPs on telomere maintenance and integrity are unknown.

During base excision repair, 8-oxoguanine DNA glycosylase (OGG1) removes 8-oxoG from the genome[20] when the damaged base pairs with cytosine, but not when it is present in single-stranded DNA or in G-quadruplex (GQ) structures[21]. Notably, an unbiased screen in yeast for genes altering telomere length has revealed that *ogg1*-deletion strains have longer telomeres than those in wild-type strains[22], and this lengthening depends partly on telomerase[23]. *Ogg1*−/− mice also have longer telomeres *in vivo*, but culturing cells from these mice in pro-oxidant conditions induces accelerated telomere shortening[10]. Thus, changes in cellular oxidative state influence telomere length. This paradox, in which 8-oxoG in telomeres promotes telomere lengthening, whereas oxidative stress causes telomere shortening, suggests a level of complexity inherent in ROS-induced DNA damage that remains unresolved.

Here we examined how the oxidized base 8-oxoG regulates telomerase activity when it is present in either the telomeric overhang or

within the dNTP pool. We found that 8-oxodGTP incorporation by telomerase terminates the chain, thereby preventing telomere restoration and promoting cell death. In contrast, the presence of a preexisting 8-oxoG in the telomeric overhang enhances telomerase activity by destabilizing the GQ structure in the folded overhang. Therefore, we demonstrate that 8-oxoG has a dual role in inhibiting or stimulating telomerase, depending on whether the free dNTPs are oxidized and inserted during extension, or the telomeric DNA is directly oxidized by free radicals.

## RESULTS

### 8-oxodGTP insertion is a telomerase chain terminator

We tested whether telomerase could introduce an 8-oxoG into telomeric DNA via utilization of 8-oxodGTP during telomere elongation. The protein component (telomerase reverse transcriptase (TERT)) catalyzes reverse transcription of an integral 11-nt RNA template located within the RNA component (TR) and adds repeats to the overhang[3]. The catalytic steps are as follows: (i) the overhang anneals to the RNA template, thus forming a short DNA–RNA hybrid that primes TERT-mediated DNA synthesis; (ii) telomerase elongates the overhang by using its template; (iii) telomerase translocates and realigns with the template, thereby priming synthesis; and (iv) cycling back to elongation generates the characteristic 6-nt-product pattern (**Fig. 1a**). The number of repeats added before telomerase dissociation determines the processivity[24].

To probe for 8-oxodGTP incorporation, we used the standard telomerase substrate of three TTAGGG repeats (3R) and examined the activity of immunopurified FLAG-tagged telomerase overexpressed in human HEK 293T cells. This well-characterized supertelomerase extract exhibits kinetic properties similar to those of endogenous telomerase[25]. We conducted reactions with widely used high dNTP concentrations and with cellular dNTP concentrations[26]. Using cellular concentrations is biologically relevant and important because the dNTP-pool balance and concentrations affect the accuracy of DNA polymerases[27]. Telomerase was similarly processive with both dNTP mixes, but the product yield was lower with the cellular dNTP mix, as observed in reactions with [α-$^{32}$P]dGTP (**Supplementary Fig. 1**). We used radiolabeled dTTP in the reactions with 8-oxodGTP. Reactions with high dNTP concentrations showed aberrant product termination after dTTP incorporation, owing to the imbalance with low dTTP. Nevertheless, increasing substitution of dGTP with 8-oxodGTP dramatically inhibited telomerase extension (**Fig. 1b** and **Supplementary Fig. 1**). The pattern of hexameric-repeat addition was restored in reactions with cellular dNTP concentrations, and the inhibitory effects of 8-oxodGTP were even more apparent (**Fig. 1b,c**). Complete substitution of dGTP with 8-oxodGTP generated a prominent band indicating termination after incorporation opposite template U and a weak band indicating incorporation opposite rC. These data suggest that telomerase can incorporate 8-oxodGTP opposite rC, albeit poorly, and that further extension from an 8-oxodGTP–C base pair is highly inhibited.

For the 3R substrate, the first repeat addition occurs opposite rArArUrC before translocation. Hence, if 8-oxodGTP is incorporated opposite rC, then further extension requires immediate translocation (**Fig. 1a**, step 3). Therefore, the problem may arise with translocation rather than extension. The GG(TTAGGG)$_2$TTAG substrate allows for 8-oxodGTP incorporation opposite cytosine (rCrCrArArUrC) and extension before translocation. Increasing substitution of 8-oxodGTP for dGTP led to dramatic telomerase inhibition, with no detectable product in reactions lacking dGTP (**Supplementary Fig. 2**). This result confirms that telomerase extension after 8-oxodGTP
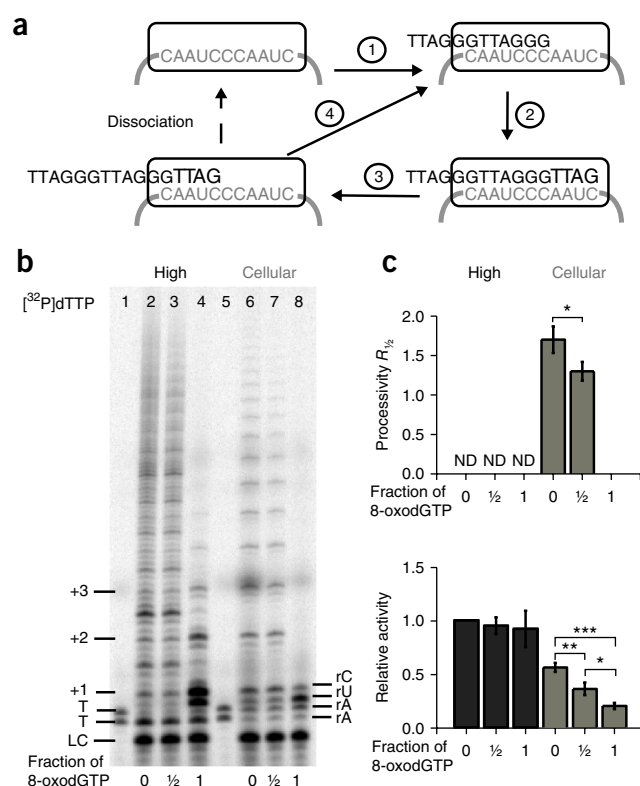


**Figure 1** 8-oxodGTP is a telomerase chain terminator. (**a**) Telomerase catalytic cycle. Larger font indicates newly added nucleotides; gray indicates the telomerase template; numbers represent steps in the cycle. (**b**) Telomerase reactions conducted with (TTAGGG)$_3$ primer (3R) with high dNTPs (500 µM dGTP, 500 µM dATP or 2.9 µM dTTP) (lanes 2–4) or cellular-concentration dNTPs (37 µM dTTP, 24 µM dATP, 29 µM dCTP or 5.2 µM dGTP) (lanes 6–8) and 0.3 µM [α-$^{32}$P]dTTP. dGTP and 8-oxodGTP were mixed at 1:0, 1:1 or 0:1 ratios for a total of 500 µM or 5.2 µM unlabeled guanine nucleotide. Products were separated on denaturing gels. The loading control (LC) was a $^{32}$P-end-labeled 18-mer oligonucleotide. Numbers on the left indicate the number of added repeats, and letters on right indicate the template base. (**c**) Processivity and relative activity, calculated on the basis of total products normalized to the LC. Data are shown as mean ± s.d. from three independent experiments. *$P < 0.05$; **$P < 0.01$; ***$P < 0.001$ by two-tailed Student's $t$ test. ND, not determined. Uncropped gel image is shown in **Supplementary Data Set 1**.

incorporation is highly unfavorable, and the lack of extension is not due to translocation inhibition.

### Telomerase incorporation of 8-oxodGTP is mutagenic

DNA polymerases can insert 8-oxodGTP opposite cytosine or adenine, although steric clashes of 8-oxodGTP–C base pairs favor insertion opposite adenine[12,28]. The accuracy of telomerase is not well established, thus raising the possibility that incorporation opposite rC might have resulted from erroneous insertion of dATP, dTTP or dCTP rather than from 8-oxodGTP insertion. To definitively test whether telomerase could incorporate 8-oxodGTP, and whether such incorporation is error prone, we radiolabeled the primer and added increasing concentrations of only dGTP or 8-oxodGTP. Reaction with a single dNTP type is a well-established method for defining polymerase fidelity (i.e., selectivity for correct rather than incorrect or damaged dNTPs) and dNTP affinity[29–31]. Unexpectedly, mutagenic incorporation opposite rA occurred even at the low concentration of 5 µM dGTP, and run-on addition occurred at high dGTP

concentrations (**Fig. 2a**). 8-oxodGTP, compared with dGTP at 5 µM, showed significantly more (50%) misinsertion opposite rA but minimal extension to the next template rA, even at high amounts (**Fig. 2b,c**). At low dNTP (5 µM), the total primers extended with 8-oxodGTP were statistically similar to extension with correct dTTP, but extension to the next rA was significantly higher for dTTP compared with mutagenic dGTP or 8-oxodGTP (**Fig. 2b,c**). All products (1 nt added and longer) required incorporation opposite the first rA. Next, we tested incorporation opposite two adjacent template rCs. Again, we observed run-on addition of dGTP incorporation beyond rC but poor incorporation and extension with 8-oxodGTP and mutagenic dATP (**Fig. 2d–f**). These data indicate that telomerase can utilize 8-oxodGTP during DNA synthesis but that it preferentially misincorporates 8-oxodGTP opposite rA versus rC, and further extension is greatly inhibited.

## Telomere dysfunction due to oxidized dNTPs

Elevating oxidized dNTPs via MTH1 depletion or inhibition causes 8-oxoG incorporation into the genome and cell death or senescence[14,32]. Cancer cells, compared with normal cells, are thought to exhibit greater sensitivity to MTH1 inhibition, as a result of a higher pro-oxidant state, but another notable difference is that most cancer cell lines depend on telomerase for proliferation[5]. Because 8-oxodGTP is a telomerase chain terminator, we reasoned that cancer cells with critically short telomeres might be the most vulnerable to telomerase inhibition. To test this possibility, we depleted MTH1 in HeLa LT cells with long telomeres (~27 kb) and HeLa VST cells with very short telomeres (~3.7 kb)[33,34] (**Supplementary Fig. 3a**). Transduction of the cells with lentiviruses expressing two distinct short hairpin RNAs (shRNAs) targeting MTH1 (sh4 and sh5) and subsequent selection with puromycin suppressed MTH1 expression by ~80–90% (**Fig. 3a**). MTH1 depletion increased nuclear 8-oxoG staining in both cell lines (**Supplementary Fig. 3c**), as has been reported for other cell lines[14,32]. These findings indicate an increase in total cellular 8-oxoG levels in nucleotide pools and incorporation into DNA.

Although oxidized dNTPs significantly inhibited proliferation of the HeLa VST cells, the HeLa LT cells were largely unaffected (**Fig. 3b**). The difference in sensitivity was not due to differences in expression of the ROS-scavenging enzymes catalase or superoxide dismutase (**Supplementary Fig. 3b**). The decreased proliferation was a result of apoptosis, as indicated by increased annexin V staining and caspase 3 cleavage in the MTH1-depleted HeLa VST cells, compared with controls, an effect that continued to day 6 after infection (**Fig. 3c–e** and **Supplementary Fig. 4a,b**). In contrast, MTH1 depletion in HeLa LT cells, compared with control cells, did not induce apoptosis (**Fig. 3c–e** and **Supplementary Fig. 4a,b**).

Next, we examined whether an increase in oxidized dNTPs would affect telomere integrity. MTH1 depletion significantly increased formation of 53BP1 foci in HeLa VST cells, as has been reported for other cell lines[14,32], but not in HeLa LT cells (**Fig. 4a–c**). 53BP1 is a DNA-damage-response protein that localizes to DNA double-strand breaks or dysfunctional telomeres; therefore, 53BP1 foci at telomeres are often referred to as telomere-dysfunction-induced foci (TIFs)[35]. MTH1 depletion in HeLa VST cells induced a six-fold increase in cells displaying three or more TIFs and in the average TIFs per nuclei, whereas HeLa LT cells were unaffected (**Fig. 4c** and **Supplementary Fig. 3e**). The number of TIFs in HeLa VST was probably underestimated, given that their very short telomeres are difficult to visualize. MTH1 depletion did not induce obvious TRF2 displacement from the telomeres (**Supplementary Fig. 3d**), a result consistent with a lack of induced telomere fusions (**Fig. 4d**). Instead, MTH1 depletion
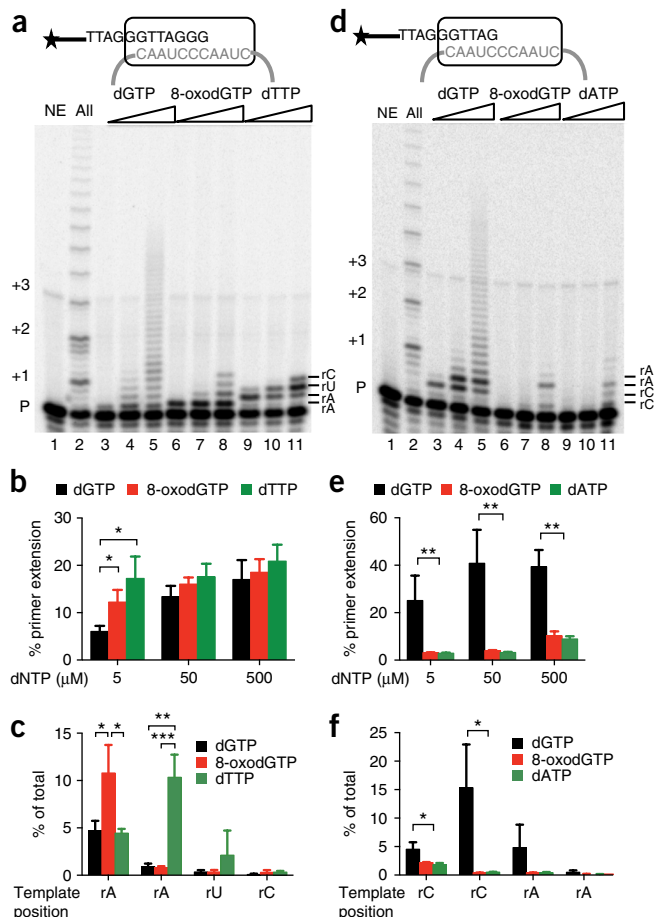


**Figure 2** Telomerase preferentially incorporates 8-oxodGTP opposite rA. (**a,d**) Telomerase activity assays conducted with 5 nM $^{32}$P-end-labeled (TTAGGG)$_3$ (**a**) or (GGTTAG)$_3$ (**d**) primers. Reactions contained cellular dNTPs (lane 2) or increasing amounts (5, 50 or 500 µM) of dGTP (lanes 3–5), 8-oxodGTP (lanes 6–8), dTTP (lanes 9–11, **a**) or dATP (lanes 9–11, **d**). Products were separated on denaturing gels. Numbers on the left indicate the number of added repeats, and letters on right indicate the template base. NE, no enzyme. (**b,e**) Percentage of total primers extended for the reactions in **a** (**b**) and **d** (**e**). (**c,f**) Percentage of primers terminated at each template position as a function of total radioactivity in the lane for the reactions in **a** (**c**) and **d** (**f**). Data are shown as mean ± s.d. from three independent experiments. *$P < 0.05$; **$P < 0.01$; ***$P < 0.001$ by two-tailed Student's $t$ test. Uncropped gel images are shown in **Supplementary Data Set 1**.

significantly increased chromatids lacking telomere staining (signal-free ends) in HeLa VST cells compared with controls, but not in HeLa LT cells (**Fig. 4d,e**). MTH1 depletion also increased fragile telomeres, as manifested as chromatid ends containing multiple telomeric signals, in the HeLa VST cells (**Fig. 4d,e**). Interestingly, the control HeLa VST cells showed more signal-free ends (or critically short telomeres) than did HeLa LT cells, but the control HeLa LT cells contained more fragile telomeres. The latter may be related to decreased TRF1 occupancy in cells with very long telomeres[36], because TRF1 prevents telomere fragility by promoting replication[37]. We passaged cells surviving after MTH1 depletion to test for effects on telomere shortening rates but found that MTH1 expression had recovered to ~30% in both cell lines and almost completely recovered in the sh5 HeLa VST (**Supplementary Fig. 3f**). These results suggest strong selective pressure for MTH1 activity after continued passaging under 20% oxygen. Our results indicate that in telomerase-expressing cancer cells,
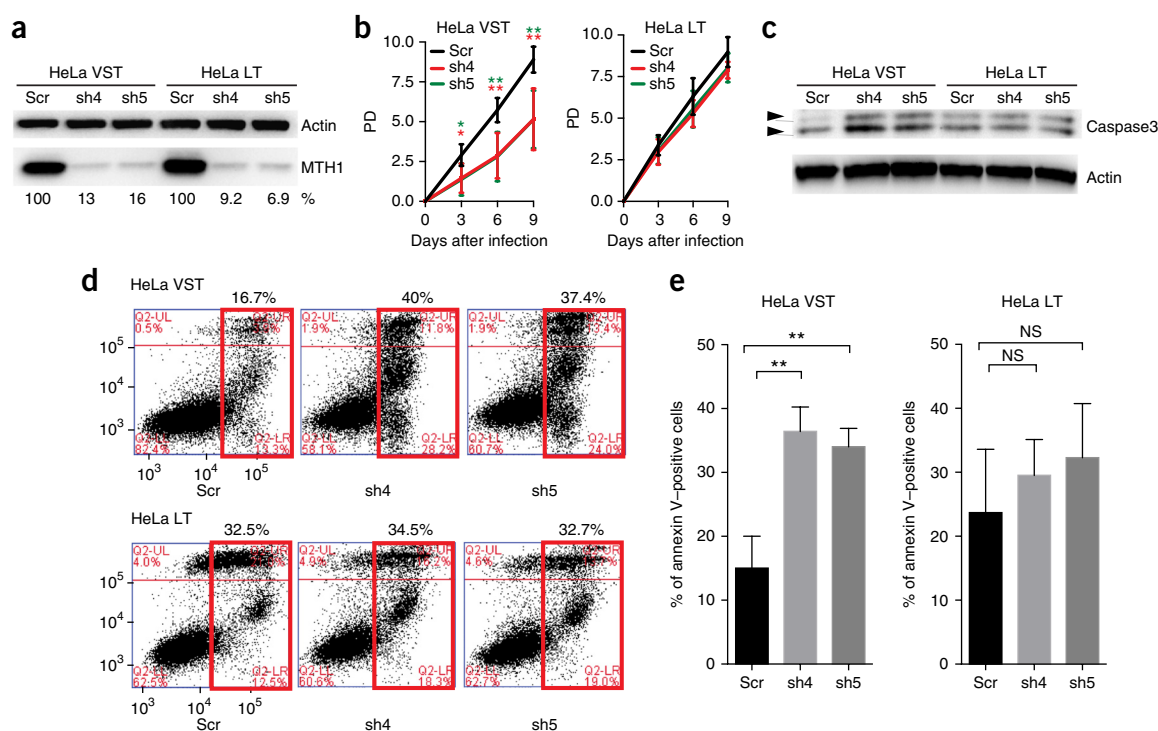
**Figure 3** Cells with shortened telomeres are hypersensitive to oxidized dNTPs. HeLa cell lines with very short telomeres (VST) or long telomeres (LT) were analyzed 3 d after transduction with lentiviruses expressing a nontargeting shRNA (scr) or different shRNAs against MTH1 (sh4 and sh5). (**a**) Immunoblot with antibodies against MTH1 or actin. The percentage MTH1 expression relative to the control was calculated. (**b**) Population-doubling (PD) values are shown as mean ± s.d. from four independent experiments. *$P < 0.05$; **$P < 0.01$ by one-way ANOVA with Tukey's honest significance difference. (**c**) Analysis of apoptosis by immunoblotting for caspase 3 activation. (**d**) Flow cytometry results of annexin V and propidium iodide staining. The numbers above the red box indicate the percentage of total annexin V– fluorescein isothiocyanate (FITC)-positive cells (both early and late apoptosis). (**e**) Quantification of percentage annexin V– FITC-positive cells. Data are shown as mean ± s.d. of 3 independent experiments *$P < 0.05$; **$P < 0.01$; NS, not significant by two-tailed Student's $t$ test. Uncropped blot images for **a** and **c** are shown in **Supplementary Data Set 1**.

the presence of shortened telomeres influences sensitivity to the adverse effects of oxidized dNTPs on cell survival and telomere integrity.

To further examine a potential role of telomerase activity in mediating sensitivity to oxidized dNTPs, in side-by-side experiments we compared MTH1 depletion in primary BJ skin fibroblasts with BJ-hTERT fibroblasts expressing exogenous telomerase. We found that, in agreement with previous work, MTH1 depletion primarily induced cell senescence in fibroblasts rather than apoptosis[32] (**Supplementary Fig. 4c** and **Supplementary Fig. 5c**). However, the BJ-hTERT cells were more sensitive than the telomerase-negative BJ cells, as evidenced by a greater induction of senescence-associated β-galatosidase activity and p53 expression, and decreased cell proliferation compared with that in controls (**Supplementary Fig. 5**). These data suggest that telomerase activity modulates cellular sensitivity to oxidized dNTPs.

**Telomerase extension from a preexisting 8-oxoG terminus**

8-oxoG can arise in the telomeric overhang through telomerase incorporation of 8-oxodGTP or by direct free-radical reaction with guanines in the overhang. We tested whether telomerase would be able to extend an overhang with a preexisting terminal 8-oxoG by using substrates of three (3R) or four (4R) TTAGGG repeats with a 3′-G or 8-oxoG (**Fig. 5a**). Telomeric overhangs in cells consist of 8–30 repeats and thus can fold into GQ structures, which impede telomerase loading[38–41]. The 3R substrate lacks sufficient sequence to form GQs and allows testing for 8-oxoG effects in the absence of structure, whereas the 4R substrate enables testing of 8-oxoG effects

in the context of biologically relevant structures. The terminal 8-oxoG substitution in 3R minimally affected telomerase processivity and total activity (**Fig. 5**), in contrast to results of experiments with 8-oxodGTP (**Fig. 1**). Telomerase also extended 3R primers when the terminal 8-oxoG aligned with rA in the template, with no significant decrease in efficiency (**Supplementary Fig. 6a–c**). These data suggest that a preexisting terminal 8-oxoG does not impair telomerase loading. The 4R substrate was poorly extended by telomerase, owing to stable GQ folding (**Fig. 5a**). Notably, the presence of a single 8-oxoG, compared with the unmodified 4R substrate, caused a dramatic restoration of processivity and activity (**Fig. 5a–c**). These data show that a preexisting terminal 8-oxoG minimally affects overhang annealing to the telomerase template in the absence of structure but highly enhances telomerase loading on the GQ-forming substrate.

Use of the 4R substrate revealed a prominent band coinciding with unextended oligonucleotides that was not visible for the 3R substrate, owing to overlap with the loading control (**Fig. 5a**, arrow). The product resulted from telomerase extension of a degraded oligonucleotide shortened to (TTAGGG)₃TTA. This result suggests that with a terminal 8-oxoG–rC base pair, the enzyme is in a nonproductive extension complex that promotes the reverse polymerase reaction, as has been described for HIV-RT[42]. The telomerase preparations lacked detectable contaminating exonuclease (**Supplementary Fig. 7a**). However, we observed enhanced degradation products on primers terminating in 8-oxoG compared with unmodified primers in telomerase reactions containing only dGTP (**Supplementary Fig. 7b,c**). This finding is consistent with our results that extension

after 8-oxodGTP incorporation opposite rC is unfavorable (**Fig. 1**). Primer degradation also occurred, but was not enhanced, when the primer 8-oxoG aligned with template rA (**Supplementary Fig. 6d,e**). This result is consistent with increased efficiency of telomerase 8-oxodGTP incorporation opposite rA versus rC (**Fig. 2**) and suggests that the 8-oxoG–rC base pair is more distorting than 8-oxoG–rA in the telomerase active site.

## 8-oxoG restores telomerase activity by disrupting G-quadruplex structure

Primer degradation and removal of the preexisting terminal 8-oxoG (**Fig. 5**) complicates interpretation of an 8-oxoG role in telomerase loading and extension. To circumvent this complication, we prepared 3R and 4R substrates with 8-oxoG substituted for the middle G of the last repeat. We did not observe any primer degradation
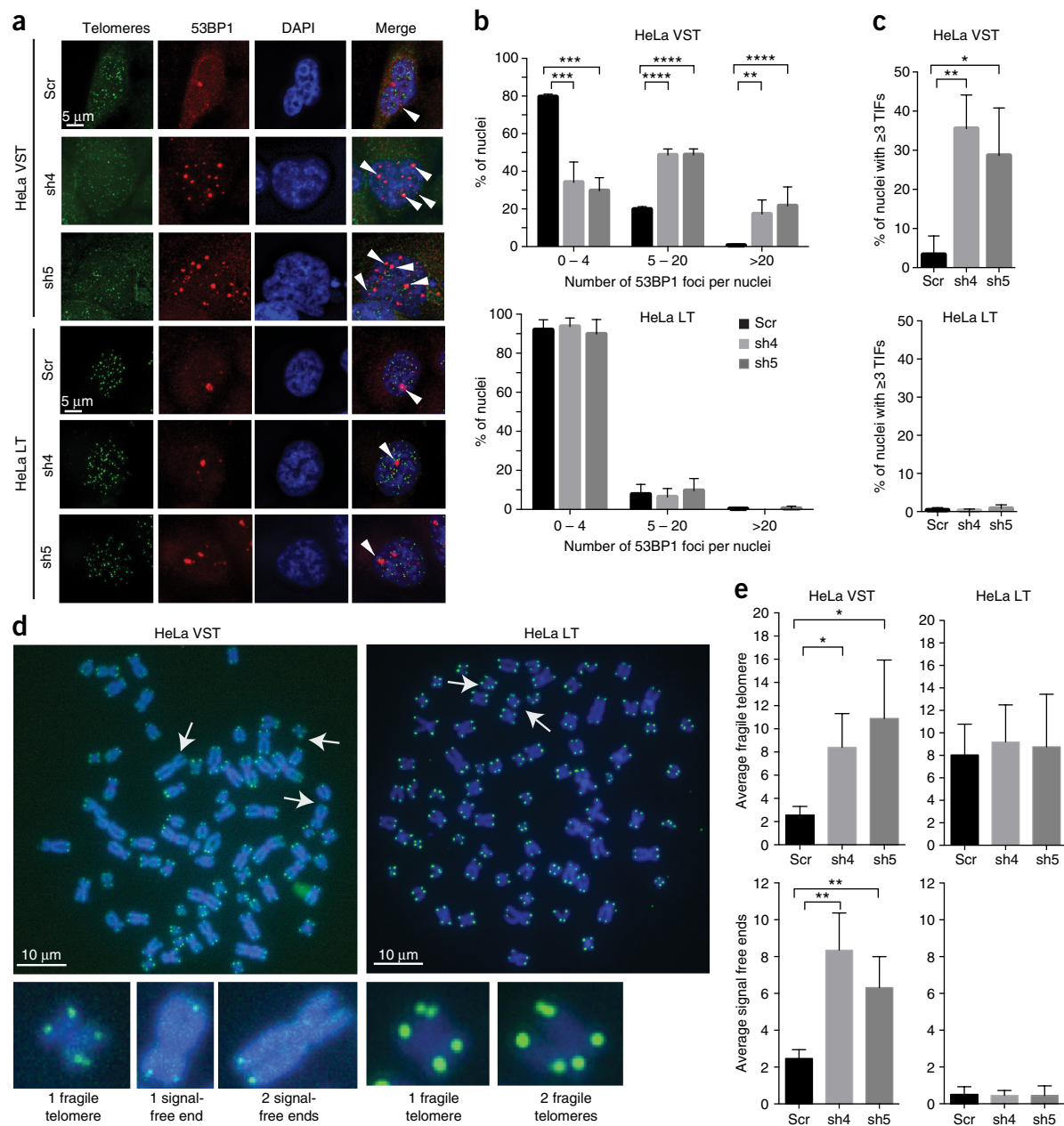


**Figure 4** Oxidized dNTPs induce telomere defects in cells with shortened telomeres. HeLa cell lines with very short telomeres (VST) or long telomeres (LT) were analyzed 3 d after transduction with lentiviruses expressing a nontargeting shRNA (scr) or different shRNAs against MTH1 (sh4 and sh5). (**a**) 53BP1 foci (red), visualized by immunofluorescence, and telomeric foci, detected by fluorescence *in situ* hybridization (green). Additional immunostaining of telomeric RAP1 protein was required in HeLa VST cells to amplify the telomere signal. 53BP1 foci at telomeres appear yellow (white arrowheads). (**b**) The number of 53BP1 foci per nuclei after binning. Data are shown as mean ± s.d. from 3 independent experiments (100–150 cells per condition). $**P < 0.01$; $***P < 0.001$; $****P < 0.0001$ by one-way ANOVA with Tukey's honest significance difference. (**c**) Percentage of nuclei showing ≥3 telomeric 53BP1 foci per nuclei (TIFs). Data are shown as mean ± s.d. from 3 independent experiments. $*P < 0.05$; $**P < 0.01$ by one-way ANOVA. (**d**) Representative metaphase chromosomes (at least 15–20 metaphases per condition) of telomere FISH from HeLa VST and HeLa LT cells expressing sh5 against MTH1. Images of fragile telomeres and signal-free ends are shown. (**e**) Quantification of telomere aberrations, average number per metaphase. Data are shown as mean ± s.d. from 3 independent experiments (at least 15–20 metaphases per condition).$*P < 0.05$; $**P < 0.01$; by two-tailed Student's *t* test.
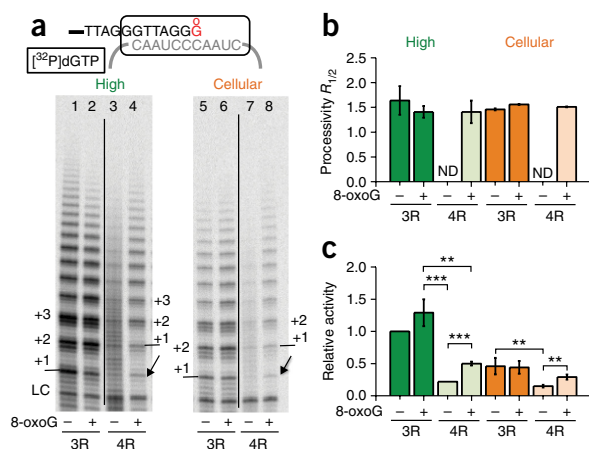
**Figure 5** Telomerase elongation of primers with a terminal 8-oxoG. (**a**) Telomerase reactions conducted with primers containing three (3R) or four (4R) TTAGGG repeats, with a 3′ terminal G or 8-oxoG (**Supplementary Table 1**, oligonucleotides 3, 4, 6 and 7). Reactions contained high (lanes 1–4) or cellular (lanes 5–8) dNTP concentrations and 0.3 μM [$\alpha$-$^{32}$P]dGTP. Telomerase products were separated on denaturing gels. The LC was $^{32}$P-end-labeled 36-mer oligonucleotide. Arrow points to a product from degraded primer. Numbers with plus signs indicate the number of added repeats. Uncropped gel image is shown in **Supplementary Data Set 1**. (**b**,**c**) Processivity and relative activity, calculated on the basis of products normalized to the LC. Data are shown as mean ± s.d. from three independent reactions. **$P < 0.01$; ***$P < 0.001$ by two-tailed Student's $t$ test. ND, not determined.



**Figure 6** 8-oxoG restores telomerase activity on quadruplex folded overhangs. (**a**) Telomerase reactions conducted with primers containing three (3R) or four (4R) TTAGGG, with a middle G or 8-oxoG (**Supplementary Table 1**, oligonucleotides 3, 5, 6 and 8). Reactions contained high (lanes 1–4) or cellular (lanes 5–8) dNTP and [$\alpha$-$^{32}$P]dGTP. Products were separated on denaturing gels. The LC was a 36-mer oligonucleotide. Numbers with plus signs indicate the number of added repeats. (**b**,**c**) Processivity (**b**) and relative activity (**c**), calculated on the basis of products normalized to the LC. Data are shown as mean ± s.d. from three independent reactions. *$P < 0.05$; **$P < 0.01$; ***$P < 0.001$ by two-tailed Student's $t$ test. ND, not determined. (**d**) Telomerase reactions with 4R primers containing a middle G or 8-oxoG in the second repeat (**Supplementary Table 1**, oligonucleotides 11 and 6). Uncropped gel images are shown in **Supplementary Data Set 1**.

products, thus indicating that the 8-oxoG remained intact, and the adjacent terminal G-rC base pair was efficiently extended (**Fig. 6a**). For the 3R substrate, the middle 8-oxoG did not affect processivity but decreased relative activity under cellular dNTP conditions (**Fig. 6b,c**). Telomerase was less sensitive to 8-oxoG with artificially high dNTPs. These studies indicate that a middle 8-oxoG may alter optimal telomerase annealing with the 3R overhang but does not interfere with extension from the G-rC base pair.

Similarly to the terminal 8-oxoG, a middle 8-oxoG in the GQ-forming substrate (4R), compared with the unmodified substrate, dramatically restored processive elongation and significantly increased telomerase activity (**Fig. 6a–c**). We obtained the same result when an 8-oxoG was inserted in the second telomeric repeat, distal from alignment with the RNA template (**Fig. 6d**). To determine the mechanism of the enhanced activity, we used a single-molecule approach that enabled probing of the GQ structure at high spatial, temporal and molecular resolution. Bulk-phase biochemical studies have indicated that telomeric DNA with 8-oxoG can fold into GQ, but the lesion lowers the GQ melting temperature[21,43]. We prepared a single-molecule fluorescence energy transfer (smFRET) reporter of telomeric GQ folding[39]. The two dyes located at both ends of the GQ-forming DNA segment with four TTAGGG repeats yielded a high-FRET peak of 0.8 in 100 mM KCl, which is indicative of compact GQ folds[39,44] (**Fig. 7a**). However, the FRET peaks for the molecules with a middle 8-oxoG in the terminal repeat shifted to a lower value indicating a less tightly folded state (**Fig. 7b**). Representative single-molecule traces of the 4R substrate displayed stable high FRET, whereas approximately 25% of the 8-oxoG molecules exhibited FRET fluctuations indicating structural dynamics (**Fig. 7c**). Dwell time determination on the basis of time spent by molecules in a low-FRET state, collected from over 300 smFRET traces revealed a dwell time of 8 s (**Fig. 7d**). To test the accessibility of
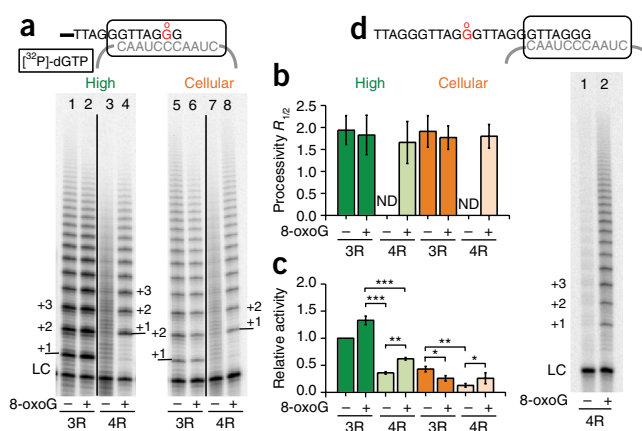
the substrates, we applied a (CCCTAA)$_4$ complementary oligonucleotide, which shifted the FRET histogram to a low-FRET peak for the 4R 8-oxoG substrate but not for the unmodified substrate (**Fig. 7e,f**). These studies strongly suggest that 8-oxoG restores telomerase activity on GQ-forming substrates by destabilizing the structure, thereby increasing telomerase accessibility and loading.

## DISCUSSION

The excess of free radicals under oxidative-stress conditions elevates oxidation of DNA and of the free-nucleotide pools. Here we found that 8-oxoG can arise in telomeres through telomerase incorporation of 8-oxodGTP, in addition to the established mechanism of telomeric DNA reacting with free radicals[45]. Our studies reveal a dual role of 8-oxoG in regulating telomerase elongation of telomeres (**Fig. 7g**). We propose that this duality leads to the paradoxical observations that under normoxic conditions unrepaired 8-oxoG lesions promote telomere lengthening, whereas oxidative stress and pro-oxidant conditions promote telomere dysfunction or shortening[6,10].

We demonstrate that 8-oxodGTP promotes chain termination after insertion by telomerase. This result suggests that perturbations at the primer terminus after damaged-nucleotide incorporation prevent the alignment of the catalytic groups and subsequent insertion and extension. Mechanistic insight into the structural changes within the active site can be gained from DNA polymerase studies that have used 8-oxoG in the template or an 8-oxodGTP inserted at the primer termini. These crystallographic studies have indicated that 8-oxoG promotes adverse changes to the nucleoside sugar pucker and phosphate backbone arising from the clash at the oxygen (O8) adduct, and insertion of 8-oxodGTP leads to an overall instability at the primer terminus and a loss of base-pairing interactions[12]. The changes are likely to promote misalignment of the primer terminus after
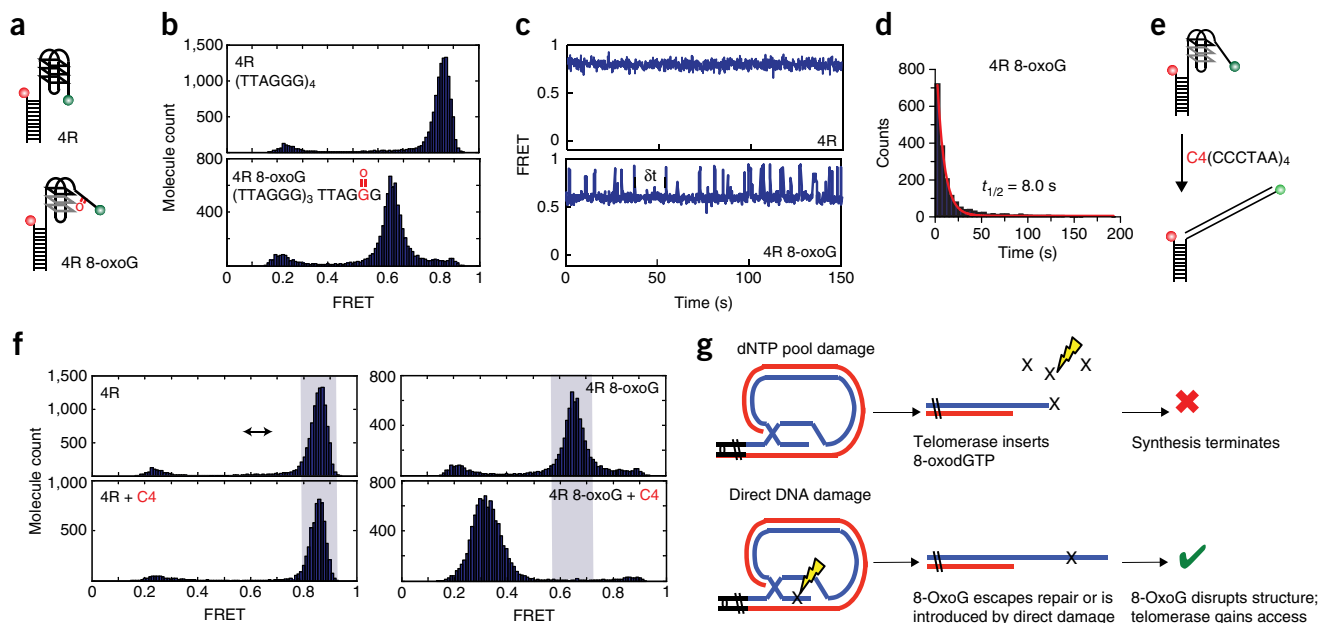
**Figure 7** 8-oxoG increases the dynamics of telomeric GQ structures. (**a**) Schematic of FRET DNA constructs for the 4R substrate with a middle G or 8-oxoG in the terminal repeat (**Supplementary Table 1**, oligonucleotides 6 and 8) with FRET-pair dyes Cy3 and Cy5 attached. (**b**) Single-molecule frequency histograms revealing FRET peaks. (**c**) Representative single-molecule traces. (**d**) The dwell time ($t_{1/2}$) calculated for the 4R substrate containing the 8-oxoG lesion. (**e**) Schematic of complementary oligonucleotide (C4) binding to the unfolded repeat. (**f**) Frequency-count histograms before and after binding of the C4 oligonucleotide to the unmodified 4R and the 8-oxoG containing 4R substrates. (**g**) Model for dual roles of 8-oxoG in regulating telomerase. Oxidation of nucleotide pools generates 8-oxodGTP, which is a telomerase chain terminator. In contrast, oxidation of the telomeric overhang promotes telomerase loading by destabilizing the GQ structure.

8-oxodGTP insertion, which then inhibits extension. This phenomenon is the basis of chain-terminating analogs, which also inhibit telomerase[46].

The result that telomerase can extend a primer with a preexisting terminal 8-oxoG (**Fig. 5**) was unexpected, given that 8-oxodGTP incorporation is chain terminating (**Fig. 1**). There are several possible explanations for this observation. First, previous studies have reported that a telomerase-associated nuclease can remove 3′ blocking nucleotides, possibly through the reverse polymerase reaction known as pyrophosphorolysis, as has been described for HIV-RT[42,47,48]. The appearance of an extended degraded primer for substrates containing a terminal 8-oxoG (**Fig. 5**) suggests that the blocking nucleotide is removed before telomerase elongation in reactions with normal dNTPs. However, if this nuclease removes 8-oxodGMP after incorporation, the presence of 8-oxodGTP in the reaction would allow reincorporation, thus setting up a futile cycle. Detection of nuclease activity depends on the ability of telomerase to elongate the substrate[47,48] (**Supplementary Figs. 6** and **7**), thus suggesting that these activities are tightly linked. Second, telomerase primer utilization may be more flexible than dNTP utilization. Previous work has shown that telomerase elongates a primer with 3′ nontelomeric sequence or a 3′-dideoxynucleotide but terminates after ddNTP incorporation[47,48]. This observation is highly reminiscent of our finding that telomerase elongates primers with a 3′-8-oxoG but fails to extend after 8-oxodGTP incorporation. The earlier studies provide evidence of a conserved telomerase endonuclease activity that can cleave primers[47,48].

The observation that 8-oxoG incorporation terminates telomerase elongation affords several predictions regarding the effects of elevating oxidized dNTPs on telomere integrity. First, telomere maintenance should be inhibited. After MTH1 depletion, the HeLa VST cells showed an average of 3.5 telomeric foci colocalized with 53BP1 (**Supplementary Fig. 3e**), an impressive result, given that telomeres

in these cells constitute less than 0.005% of the genome. The TIFs are probably underestimated, given that very short telomeres are difficult to detect. Moreover, MTH1 depletion also increased telomere loss in HeLa VST cells (**Fig. 4d,e**). Although reliable methods for precisely measuring 8-oxodGTP levels are lacking, even trace amounts of 8-oxodGTP (<1% of dGTP) cause DNA polymerase γ to generate mutations[49]. Replicative polymerases have much lower error rates ($\sim10^{-6}$) than that of telomerase ($\sim10^{-3}$)[50,51], and the observation that high-fidelity polymerases utilize 8-oxodGTP in cells[16,28] suggests that telomerase may do so as well. Second, MTH1 depletion should accelerate telomere shortening. Unfortunately, the recovery of MTH1 expression during continued cell culturing precluded the determination of effects on telomere shortening, thus suggesting that there was selective pressure for MTH1 expression during passaging under 20% oxygen. Third, the deleterious effects of MTH1 depletion should depend partly on telomerase activity. BJ-hTERT fibroblasts are more sensitive than telomerase-deficient BJ cells (**Supplementary Fig. 5**). Previous studies have also reported that telomerase-deficient primary cells are less sensitive to MTH1 inhibitors than cancer cell lines, almost all of which are telomerase positive[14]. Tumors frequently have shortened telomeres despite the presence of telomerase[52]. Whether the telomerase-negative U2OS cancer cell line, which maintains telomeres by alternative lengthening of telomeres, is sensitive to MTH1 inhibitors is controversial[14,53]. Collectively, these studies indicate that dependence on robust telomerase activity may partly explain why cancer cells are more sensitive than normal cells to oxidized dNTPs.

The finding that cancer cells with short telomeres are more sensitive to MTH1 depletion than cells with long telomeres suggests a difference in the dependence on telomerase activity for short-term viability. In agreement with this possibility, previous studies have found that cancer cells with short telomeres are more sensitive to telomerase

inhibition than cancer cells with long telomeres, and that apoptosis induction is rapid, within 2–4 d (refs. 41,54), similarly to MTH1 depletion in HeLa VST cells. This timing is insufficient to allow enough cell divisions for substantial telomere shortening, thus supporting the model in which cells with short telomeres replicate with critically short telomeres and require telomerase activity at each cycle for viability[54]. In agreement with this possibility, control HeLa VST cells have more telomeric signal-free ends than do HeLa LT cells (**Fig. 4e**). Similarly to our results with MTH1 depletion, treating telomerase-positive cancer cells with the analog 6-thio-2′-deoxyguanosine (6-thio-dG) also induces rapid cell death and acute telomere dysfunction[55]. Normal telomerase-deficient cells are less sensitive to 6-thio-dG, similarly to their lower sensitivity to oxidized dNTPs[14,55]. Collectively, these results indicate that cancer cells with limited telomere reserves are vulnerable to acute telomerase inhibition by the incorporation of chain-terminating nucleotides.

Our result that 8-oxoG destabilizes GQs in the telomeric overhang and enhances telomerase accessibility (**Figs. 5–7**), offers an explanation for the findings that unrepaired 8-oxoG lesions in OGG1-deficient mice and yeast promote telomere lengthening *in vivo* or cell culturing under 3% oxygen[10,23]. Although OGG1 cannot remove 8-oxoG in single-stranded DNA, it can do so when the overhang pairs with duplex DNA in the t loop–D loop structure[56]. Interestingly, culturing OGG1-deficient cells under 20% oxygen promotes telomere shortening and aberrations[10], thus suggesting that under pro-oxidant conditions, MTH1 levels in normal cells are insufficient to sanitize dNTP pools[32]. Our studies indicate that the elevated levels of oxidized dNTPs caused by oxidative stress probably contribute to telomere shortening in OGG1-deficient cells cultured under pro-oxidant conditions and override any benefits of 8-oxoG destabilization of telomeric GQ.

Our results indicate that addiction to MTH1 in cancer cells is modulated partly by their telomere length and their dependence on robust telomerase activity for short-term viability. Whereas incorporation of oxidized nucleotides might also affect shelterin binding or t-loop assembly, such effects are inconsistent with the lack of sensitivity to MTH1 depletion observed in HeLa cells with long telomeres. Thus, the analysis of telomere length in telomerase-positive tumors may predict which tumors would be responsive to MTH1 inhibition. A recent study has reported that human U2OS and SW480 cell lines are insensitive to MTH1 depletion[53], thus further suggesting that numerous cellular factors influence sensitivity to oxidized dNTPs. For example, MTH1 depletion in cells expressing oncogenic RAS suppresses transformation and tumorigenesis[17,57]. Finally, antioxidant therapy promotes metastasis of human melanoma in mouse models, thus suggesting that oxidative stress may inhibit metastatic progression *in vivo*[58]. Our studies provide evidence that oxidative-stress-induced damage of dNTP pools inhibits the ability of telomerase to maintain telomeres for sustained proliferation of malignant cells with critically short telomeres.

## METHODS

Methods, including statements of data availability and any associated accession codes and references, are available in the online version of the paper.

*Note: Any Supplementary Information and Source Data files are available in the online version of the paper.*

## AUTHOR CONTRIBUTIONS

E.F., J. Lormand and A.B. performed biochemical and cellular experiments, analyzed the data and prepared figures. H.-T.L. and G.S.K. performed all the smFRET studies. J. Li and R.W.S. provided lentiviruses for MTH1 depletion experiments, and R.W.S. provided helpful discussions. E.F., B.D.F., S.M. and P.L.O. designed experiments, analyzed the data and wrote the manuscript.

1. Jaskelioff, M. *et al.* Telomerase reactivation reverses tissue degeneration in aged telomerase-deficient mice. *Nature* **469**, 102–106 (2011).
2. Armanios, M. & Blackburn, E.H. The telomere syndromes. *Nat. Rev. Genet.* **13**, 693–704 (2012).
3. Greider, C.W. & Blackburn, E.H. A telomeric sequence in the RNA of *Tetrahymena* telomerase required for telomere repeat synthesis. *Nature* **337**, 331–337 (1989).
4. Hockemeyer, D. & Collins, K. Control of telomerase action at human telomeres. *Nat. Struct. Mol. Biol.* **22**, 848–852 (2015).
5. Kim, N.W. *et al.* Specific association of human telomerase activity with immortal cells and cancer. *Science* **266**, 2011–2015 (1994).
6. von Zglinicki, T. Oxidative stress shortens telomeres. *Trends Biochem. Sci.* **27**, 339–344 (2002).
7. Jurk, D. *et al.* Chronic inflammation induces telomere dysfunction and accelerates ageing in mice. *Nat. Commun.* **2**, 4172 (2014).
8. Lonkar, P. & Dedon, P.C. Reactive species and DNA damage in chronic inflammation: reconciling chemical mechanisms and biological fates. *Int. J. Cancer* **128**, 1999–2009 (2011).
9. Poljšak, B. & Fink, R. The protective role of antioxidants in the defence against ROS/RNS-mediated environmental pollution. *Oxid. Med. Cell. Longev.* **2014**, 671539 (2014).
10. Wang, Z. *et al.* Characterization of oxidative guanine damage and repair in mammalian telomeres. *PLoS Genet.* **6**, e1000951 (2010).
11. Kamiya, H. & Kasai, H. Formation of 2-hydroxydeoxyadenosine triphosphate, an oxidatively damaged nucleotide, and its incorporation by DNA polymerases: steady-state kinetics of the incorporation. *J. Biol. Chem.* **270**, 19446–19450 (1995).
12. Freudenthal, B.D. *et al.* Uncovering the polymerase-induced cytotoxicity of an oxidized nucleotide. *Nature* **517**, 635–639 (2015).
13. Tsuzuki, T. *et al.* Spontaneous tumorigenesis in mice defective in the MTH1 gene encoding 8-oxo-dGTPase. *Proc. Natl. Acad. Sci. USA* **98**, 11456–11461 (2001).
14. Gad, H. *et al.* MTH1 inhibition eradicates cancer by preventing sanitation of the dNTP pool. *Nature* **508**, 215–221 (2014).
15. Sakumi, K. *et al.* Cloning and expression of cDNA for a human enzyme that hydrolyzes 8-oxo-dGTP, a mutagenic substrate for DNA synthesis. *J. Biol. Chem.* **268**, 23524–23530 (1993).
16. Speina, E. *et al.* Contribution of hMTH1 to the maintenance of 8-oxoguanine levels in lung DNA of non-small-cell lung cancer patients. *J. Natl. Cancer Inst.* **97**, 384–395 (2005).
17. Patel, A. *et al.* MutT Homolog 1 (MTH1) maintains multiple KRAS-driven pro-malignant pathways. *Oncogene* **34**, 2586–2596 (2015).
18. Liou, G.Y. & Storz, P. Reactive oxygen species in cancer. *Free Radic. Res.* **44**, 479–496 (2010).
19. Szatrowski, T.P. & Nathan, C.F. Production of large amounts of hydrogen peroxide by human tumor cells. *Cancer Res.* **51**, 794–798 (1991).
20. Wallace, S.S. Base excision repair: a critical player in many games. *DNA Repair (Amst.)* **19**, 14–26 (2014).
21. Zhou, J., Liu, M., Fleming, A.M., Burrows, C.J. & Wallace, S.S. Neil3 and NEIL1 DNA glycosylases remove oxidative damages from quadruplex DNA and exhibit preferences for lesions in the telomeric sequence context. *J. Biol. Chem.* **288**, 27263–27272 (2013).
22. Askree, S.H. *et al.* A genome-wide screen for *Saccharomyces cerevisiae* deletion mutants that affect telomere length. *Proc. Natl. Acad. Sci. USA* **101**, 8658–8663 (2004).
23. Lu, J. & Liu, Y. Deletion of Ogg1 DNA glycosylase results in telomere base damage and length alteration in yeast. *EMBO J* **29**, 398–409 (2010).
24. Schmidt, J.C. & Cech, T.R. Human telomerase: biogenesis, trafficking, recruitment, and activation. *Genes Dev.* **29**, 1095–1105 (2015).

25. Xi, L. & Cech, T.R. Inventory of telomerase components in human cells reveals multiple subpopulations of hTR and hTERT. *Nucleic Acids Res.* **42**, 8565–8577 (2014).

26. Traut, T.W. Physiological concentrations of purines and pyrimidines. *Mol. Cell. Biochem.* **140**, 1–22 (1994).

27. Sohl, C.D., Ray, S. & Sweasy, J.B. Pools and Pols: mechanism of a mutator phenotype. *Proc. Natl. Acad. Sci. USA* **112**, 5864–5865 (2015).

28. Katafuchi, A. & Nohmi, T. DNA polymerases involved in the incorporation of oxidized nucleotides into DNA: their efficiency and template base preference. *Mutat. Res.* **703**, 24–31 (2010).

29. Hsu, G.W., Ober, M., Carell, T. & Beese, L.S. Error-prone replication of oxidatively damaged DNA by a high-fidelity DNA polymerase. *Nature* **431**, 217–221 (2004).

30. Bertram, J.G., Oertell, K., Petruska, J. & Goodman, M.F. DNA polymerase fidelity: comparing direct competition of right and wrong dNTP substrates with steady state and pre-steady state kinetics. *Biochemistry* **49**, 20–28 (2010).

31. Tomlinson, C.G. *et al.* Two-step mechanism involving active-site conformational changes regulates human telomerase DNA binding. *Biochem. J.* **465**, 347–357 (2015).

32. Rai, P. *et al.* Continuous elimination of oxidized nucleotides is necessary to prevent rapid onset of cellular senescence. *Proc. Natl. Acad. Sci. USA* **106**, 169–174 (2009).

33. Crabbe, L., Cesare, A.J., Kasuboski, J.M., Fitzpatrick, J.A. & Karlseder, J. Human telomeres are tethered to the nuclear envelope during postmitotic nuclear assembly. *Cell Rep.* **2**, 1521–1529 (2012).

34. O'Sullivan, R.J. *et al.* Rapid induction of alternative lengthening of telomeres by depletion of the histone chaperone ASF1. *Nat. Struct. Mol. Biol.* **21**, 167–174 (2014).

35. Takai, H., Smogorzewska, A. & de Lange, T. DNA damage foci at dysfunctional telomeres. *Curr. Biol.* **13**, 1549–1556 (2003).

36. Takai, K.K., Hooper, S., Blackwood, S., Gandhi, R. & de Lange, T. *In vivo* stoichiometry of shelterin components. *J. Biol. Chem.* **285**, 1457–1467 (2010).

37. Sfeir, A. *et al.* Mammalian telomeres resemble fragile sites and require TRF1 for efficient replication. *Cell* **138**, 90–103 (2009).

38. Biffi, G., Tannahill, D., McCafferty, J. & Balasubramanian, S. Quantitative visualization of DNA G-quadruplex structures in human cells. *Nat. Chem.* **5**, 182–186 (2013).

39. Hwang, H. *et al.* Telomeric overhang length determines structural dynamics and accessibility to telomerase and ALT-associated proteins. *Structure* **22**, 842–853 (2014).

40. Zahler, A.M., Williamson, J.R., Cech, T.R. & Prescott, D.M. Inhibition of telomerase by G-quartet DNA structures. *Nature* **350**, 718–720 (1991).

41. Cookson, J.C. *et al.* Pharmacodynamics of the G-quadruplex-stabilizing telomerase inhibitor 3,11-difluoro-6,8,13-trimethyl-8H-quino[4,3,2-kl]acridinium methosulfate (RHPS4) *in vitro*: activity in human tumor cells correlates with telomere length and can be enhanced, or antagonized, with cytotoxic agents. *Mol. Pharmacol.* **68**, 1551–1558 (2005).

42. Meyer, P.R., Matsuura, S.E., So, A.G. & Scott, W.A. Unblocking of chain-terminated primer by HIV-1 reverse transcriptase through a nucleotide-dependent mechanism. *Proc. Natl. Acad. Sci. USA* **95**, 13471–13476 (1998).

43. Vorlíčková, M., Tomasko, M., Sagi, A.J., Bednarova, K. & Sagi, J. 8-oxoguanine in a quadruplex of the human telomere DNA sequence. *FEBS J.* **279**, 29–39 (2012).

44. Tippana, R., Xiao, W. & Myong, S. G-quadruplex conformation and dynamics are determined by loop length and sequence. *Nucleic Acids Res.* **42**, 8106–8114 (2014).

45. Oikawa, S., Tada-Oikawa, S. & Kawanishi, S. Site-specific DNA damage at the GGG sequence by UVA involves acceleration of telomere shortening. *Biochemistry* **40**, 4763–4768 (2001).

46. Hukezalie, K.R., Thumati, N.R., Côté, H.C. & Wong, J.M. *In vitro* and *ex vivo* inhibition of human telomerase by anti-HIV nucleoside reverse transcriptase inhibitors (NRTIs) but not by non-NRTIs. *PLoS One* **7**, e47505 (2012).

47. Oulton, R. & Harrington, L. A human telomerase-associated nuclease. *Mol. Biol. Cell* **15**, 3244–3256 (2004).

48. Huard, S. & Autexier, C. Human telomerase catalyzes nucleolytic primer cleavage. *Nucleic Acids Res.* **32**, 2171–2180 (2004).

49. Pursell, Z.F., McDonald, J.T., Mathews, C.K. & Kunkel, T.A. Trace amounts of 8-oxo-dGTP in mitochondrial dNTP pools reduce DNA polymerase gamma replication fidelity. *Nucleic Acids Res.* **36**, 2174–2181 (2008).

50. Kunkel, T.A. DNA replication fidelity. *J. Biol. Chem.* **279**, 16895–16898 (2004).

51. Kreiter, M., Irion, V., Ward, J. & Morin, G. The fidelity of human telomerase. *Nucleic Acids Symp. Ser.* 137–139 (1995).

52. Bisoffi, M., Heaphy, C.M. & Griffith, J.K. Telomeres: prognostic markers for solid tumors. *Int. J. Cancer* **119**, 2255–2260 (2006).

53. Kettle, J.G. *et al.* Potent and selective inhibitors of MTH1 probe its role in cancer cell survival. *J. Med. Chem.* **59**, 2346–2361 (2016).

54. Zhang, X., Mar, V., Zhou, W., Harrington, L. & Robinson, M.O. Telomere shortening and apoptosis in telomerase-inhibited human tumor cells. *Genes Dev.* **13**, 2388–2399 (1999).

55. Mender, I., Gryaznov, S., Dikmen, Z.G., Wright, W.E. & Shay, J.W. Induction of telomere dysfunction mediated by the telomerase substrate precursor 6-thio-2'-deoxyguanosine. *Cancer Discov.* **5**, 82–95 (2015).

56. Rhee, D.B., Ghosh, A., Lu, J., Bohr, V.A. & Liu, Y. Factors that influence telomeric oxidative base damage and repair by DNA glycosylase OGG1. *DNA Repair (Amst)* **10**, 34–44 (2011).

57. Giribaldi, M.G., Munoz, A., Halvorsen, K., Patel, A. & Rai, P. MTH1 expression is required for effective transformation by oncogenic HRAS. *Oncotarget* **6**, 11519–11529 (2015).

58. Piskounova, E. *et al.* Oxidative stress inhibits distant metastasis by human melanoma cells. *Nature* **527**, 186–191 (2015).

# ONLINE METHODS

**Cell culture and lentiviral infection.** HEK-293T cells, BJ skin fibroblasts (CL-5222) and BJ-5ta skin fibroblasts expressing hTERT (CRL-4001) were from ATCC, and HeLa VST and HeLa LT cells were a generous gift from R. O'Sullivan (University of Pittsburgh). Cells were cultured in DMEM supplemented with 10% FBS, 50 units/ml penicillin and 50 units/ml streptomycin (Gibco) at 37 °C in humidified chambers under 5% $CO_2$ and 20% $O_2$. The Gibco FBS was replaced with characterized FBS from Hyclone for culturing BJ and BJ-hTERT cells. Mycoplasma testing was performed routinely through DAPI staining and was followed by PCR assays when required (Venor GeM Mycoplasma Detection Kit, Sigma-Aldrich). MTH1-knockdown cell lines were established by overnight transduction with lentivirus-expressing shRNAs (sh4 or sh5) targeting MTH1 transcript or a nontargeting scrambled shRNA (scr). Selection of transduced cells was performed with 1.5 µg/ml puromycin (HeLa VST and HeLa LT) or 0.75 µg/ml puromycin (BJ and BJ-hTERT) after 24 h of recovery. Lentiviral particles were generated by cotransfection of 4 plasmids (control plasmid (pLKO.1-SCRshRNA-Puro) or one of the five different MTH1-specific shRNA–expressing plasmids, pLKO.1-shRNA-MTH1.1–MTH1.5) together with pMD2.g (VSVG), pVSV-REV and pMDLg/pRRE) into 293-FT cells with a *TransIT*-X2Dynamic Delivery System (Mirus Bio) with support from the University of South Alabama Mitchell Cancer Institute (USA/MCI) Gene Expression, Editing and Discovery (GEED) Lab. The lentiviruses were further concentrated with a Lenti-X Concentrator (Clontech), per the manufacturer's instructions. Five different shRNAs targeting the MTH1 gene were initially screened, and clone IDs (sh#4) NM_002452.3-96s1c1 and (sh#5) NM_002452.3-96s21c1 (Sigma) were the most effective (data not shown). The collection and isolation of lentiviral particles and the transduction of cells described in the text were performed as previously described[59].

**Telomerase preparation.** Telomerase was immunopurified as previously described[39]. Cells expressing hTR and 3×FLAG-tagged hTERT were harvested 48 h after transfection and lysed in CHAPS lysis buffer (10 mM Tris-HCl, 1 mM MgCl$_2$, 1 mM EDTA, 0.5% CHAPS, 10% glycerol, 5 mM β-mercaptoethanol, 120 U RNasin Plus (Promega), 1 µg/ml each of pepstatin, aprotinin, leupeptin and chymostatin, and 1 mM AEBSF) for 30 min at 4 °C. Sigma anti-FLAG M2 affinity gel agarose beads (75 µl of a 1:1 slurry) were prewashed with 1× human telomerase buffer (50 mM Tris-HCl, pH 8, 50 mM KCl, 1 mM MgCl$_2$, 1 mM spermidine and 5 mM β-mercaptoethanol) with 30% glycerol and mixed with 500 µl of cell lysate for 3 h at 4 °C with rotation. Beads were harvested by centrifugation at 3,500 r.p.m. for 1 min, washed three times with 1× telomerase buffer with 30% glycerol, flash frozen as a 1:1 slurry in 1× telomerase buffer with 30% glycerol and stored at −80 °C.

**Telomerase activity assay.** Telomerase overexpression in HEK-293T cells was achieved by transient transfection with plasmids expressing hTR and 3×FLAG-tagged hTERT (a gift from T. Cech). Cells were grown to 90% confluency and transfected with Lipofectamine 2000 reagent (Invitrogen), and telomerase was immunopurified as previously described[39]. Unmodified oligonucleotides were from IDT, and oligonucleotides with 8-oxoG were from Midland Certified Reagents Company (**Supplementary Table 1**). The telomerase assay was as previously described[39,60]. Briefly, reactions (20 µl) contained 1× human telomerase buffer, 1 µM oligonucleotide substrate, 0.3 µM of 3,000 Ci/mmol [α-$^{32}$P]dGTP or [α-$^{32}$P]dTTP (PerkinElmer) and dNTP (Invitrogen) mix, as indicated in the figure legends. Reactions with high dNTPs contained either (500 µM dTTP, 500 µM dATP, 2.9 µM dGTP and 0.3 µM [α-$^{32}$P]dGTP) or (500 µM dGTP, 500 µM dATP, 2.9 µM dTTP and 0.3 µM [α-$^{32}$P]dTTP). Reactions with cellular dNTPs contained 37 µM dTTP, 24 µM dATP, 29 µM dCTP, 5.2 µM dGTP and 0.3 µM [α-$^{32}$P]dGTP or [α-$^{32}$P]dTTP as indicated. Reactions containing 8-oxo-dGTP (TriLink Biotechnologies) substituted for dGTP are indicated in the figure legends. For reactions with end-labeled primers, the primers were labeled with [γ-$^{32}$P]ATP (PerkinElmer) and 10 U Optikinase (Affymetrix) according to the manufacturers' protocols. Reactions contained 1× telomerase buffer, 5 nM of $^{32}$P-end-labeled primer and cellular dNTP mix or dGTP, 8-oxodGTP, dTTP or dATP (5.2 µM, 50 µM or 500 µM), as indicated in the figure legends. Reactions were started by addition of 6 µl of immunopurified telomerase slurry, incubated for 1 h at 30 °C, then terminated with 2 µl of 0.5 µM EDTA and heat inactivated at 65 °C for 20 min. For reactions with unlabeled primers, 8.0 fmol of $^{32}$P-end-labeled loading control (LC) was added to the inactivated reaction before purification

with an Illustra Microspin G-25 column (GE Healthcare). After addition of an equal volume of loading dye, the samples were heat-denatured and then loaded onto a 10% denaturing acrylamide gel (8 M urea and 1× TBE) for electrophoresis. Samples were imaged with a Typhoon phosphorimager (GE Healthcare). Telomerase processivity and relative telomerase activity was quantified with ImageQuant and normalized to the LC as previously described[60]. The processivity factor $R_{1/2}$ is the number of repeats that telomerase adds before half of the DNA substrates dissociate from the enzyme. For reactions with end-labeled primers, the products were quantified with ImageQuant by measuring the intensity of each product band and dividing by the total radioactivity in the lane.

**Annexin V–propidium iodide apoptosis assay.** The assay was conducted with an Annexin V–FITC Apoptosis Detection Kit (Abcam) according to the manufacturer's directions. Cells were seeded at $4 \times 10^5$ cells in 60-mm dishes at least 24 h before infection with lentiviruses. On day three after lentiviral infection, cells were trypsinized and counted. $3 \times 10^5$ cells were harvested by centrifugation for 5 min at 1,200 r.p.m. and then washed once with PBS. Cells were resuspended in 500 µl binding buffer (provided in the kit) containing 5 µl annexin V–FITC and 5 µl of propidium iodide (50 µg/ml). Cells were incubated in the dark for 5 min at room temperature. FL1 and FL2 emission was measured with an Accuri C6 flow cytometer after application of color compensation.

**Western blots.** Cells were resuspended in 400 mM NaCl buffer, and whole cell extracts were prepared by freeze-thaw cycles, then centrifuged 15 min at 14,000 r.p.m. Protein amounts were measured with Bradford reagent (Sigma). MTH1 (1:5,000, Abcam, ab200832), β-actin (1:10,000, Sigma, A5441), caspase 3 (1:500, Cell Signaling, 9664S), SOD (1:2,000, Abcam, ab13498), catalase (1:2,000, Abcam, ab16731) and p53 (1:1,000, Santa Cruz, DO-1) antibodies were used. Validation is provided on the manufacturers' websites.

**Immunofluorescence and fluorescence *in situ* hybridization.** Cells were grown on Mattek glass-bottom dishes and fixed in 4% formaldehyde for 10 min at room temperature, except for TRF2 immunostaining, cells were fixed on ice in 2% formaldehyde. After being washed three times with PBS, cells were then washed three times for 5 min each in PBS containing 0.2% Triton X-100 and blocked for 1 h in blocking solution (10% goat serum and Validation is provided on the manufacturers' websites. 1% BSA in PBS). Mouse monoclonal 53BP1 antibody (1:500 dilution, Millipore, MAB3804) or TRF2 monoclonal antibody (1:250 dilution, 4A794.15, Novus) was added and incubated at 4 °C overnight. For the HeLa VST cells, the 53BP1 antibody mix also contained the rabbit RAP1 polyclonal antibody (1:500 dilution, Bethyl laboratories, A300-306A) to amplify the telomere signal. Cells were washed in PBS three times for 10 min each at room temperature with mild shaking and incubated with secondary antibody (1:1,000 dilution, goat anti-mouse Alexa 594 (Life Technologies, A11005) for HeLa LT; a mix of anti-mouse Alexa 594 and goat anti-rabbit Alexa 488 (Life Technologies, A1108) for HeLa VST; or a 1:500 dilution of anti-mouse Alexa 594 for TRF2 immunostaining) for 1 h. After being washed three times in PBS, cells were fixed in methanol/acetone 1:1 (v/v) at −20 °C for 10 min, or in 2% formaldehyde for 10 min at room temperature for TRF2 immunostaining, and dehydrated in 70%, 90% and 100% ethanol for 5 min. 100 mg/ml telomeric γPNA probe (H$_2$N-Lys-(AATCCC)$_2$-FITC, PNA Innovations[61]) was diluted 1:500 in hybridization buffer (70% formamide, 10 mM Tris-HCl, pH 7.5, 1× maleic acid buffer, 1× MgCl$_2$ buffer) and boiled for 5 min at 95 °C. Samples were incubated for 10 min on a hot plate at 75 °C and then at room temperature for 2 h in the dark. After being washed twice in hybridization wash buffer (70% formamide, 10 mM Tris-HCl, pH 7.5), slides were mounted with Antifade Gold containing DAPI. Imaging acquisition was performed with a Nikon Ti inverted fluorescence microscope. Z stacks of 0.2-µm thickness were captured, and images were deconvolved with the NIS Elements Advance Research software algorithm. Wide-field imaging with deconvolution, in this case with blind, iterative methods, offered the advantage of minimizing signal loss and was critical for imaging the dim shortened telomeres in the HeLa VST cells. Validation of the primary and secondary antibodies is provided on the manufacturers' websites.

**Chromosome metaphase preparation and telomere FISH.** Telomere FISH of metaphase chromosome preparations was performed as previously described. Briefly, 3 d after lentiviral transduction, cells were treated with 0.05 µg/ml colcemid

for 2 h. Cells ($1 \times 10^6$ at a density of $1 \times 10^5$ cell/ml) were harvested and incubated with 75 mM KCl hypotonic buffer for 7 min at 37 °C, then fixed in methanol/acetic acid (3:1). Samples were stored at −20 °C. Lysed cells were dropped onto water-coated glass microscope slides and dried at room temperature overnight. The slides were then fixed in 4% formaldehyde, washed with PBS and then treated with 0.25 mg/ml RNase A for 15 min at 37 °C. Next, the slides were incubated with 1 mg/ml pepsin in 0.01 N HCl for 15 min at 37 °C. Fixation and washing were repeated. Slides were then dehydrated in successive ethanol solutions of 70%, 90%, and 100% for 5 min each and allowed to dry overnight or for at least 3 h on at room temperature. Telomere FISH with a FITC-conjugated telomeric PNA probe was conducted, and images were captured and analyzed as described above.

**Measurement of colocalized 53BP1 and telomeric foci.** The numbers of 53BP1 foci and intersection with telomeres were counted per nuclei with NIS Element Advanced Research software (Nikon) after deconvolution. Briefly, the measurement feature of the software was used to create binary layers on the basis of intensity and defining binary objects corresponding to 53BP1 foci and telomere foci. An intensity threshold was set up for an image from the control experiment (scr) for each channel (threshold FITC for telomeres and threshold Cy3 for 53BP1) and held constant for analysis of images from the MTH1-depleted cells (sh4 and sh5). The binary objects corresponding to areas smaller than 0.05 µm were discarded. The intersection tool was then used to create a third binary layer corresponding to the 53BP1 binary objects overlapping with telomere binary objects. Nuclei were isolated with region of interest (ROI) identification tools on the basis of DAPI staining, and the numbers of 53BP1 foci and intersections per ROI were exported in excel for data batch analysis.

**Immunodetection of 8oxoG by immunofluorescence.** Nuclear 8oxoG immunodetection was performed as previously described[62] with monoclonal mouse antibody (Millipore MAB3560) diluted 1:50 in goat anti-mouse IgM.

**Southern blotting.** Measurements of telomere length in HeLa VST and HeLa LT were performed as previously described[63,64] with slight modifications. Briefly, 3 µg of genomic DNA was digested with a cocktail of four restriction enzymes (RsaI, AluI, HindIII and MnlI) for 16 h at 37 °C and resolved on an 0.8% agarose gel for 16 h 30 min (HeLa VST) or 24 h (HeLa LT). The agarose gel was dried for 2 h at 50 °C, and radioactive telomeric probe was hybridized overnight at 42 °C.

**Senescence-associated β-galactosidase assay.** A Cellular Senescence Assay Kit (Cell BioLabs) was used to detect the senescence-associated β-galactosidase activity in cells 3 d after lentiviral infection. The staining was carried out in 35-mm dishes overnight at 37 °C, per the manufacturer's instructions. For quantification, at least 100 cells, spanning four or five microscopy fields, were scored for staining with a 20× objective and a light microscope.

**Preparation of oligonucleotides for SM FRET.** DNA oligonucleotides used in single-molecule fluorescence experiments were 5′ TGG CGA CGG CAG CGA GGC (TTA GGG)$_4$-Cy3 (oligonucleotide 6; **Supplementary Table 1**), TGG CGA CGG CAG CGA GGC (TTAGGG)$_3$TTAG(8-oxo-dG)G-Cy3 (oligonucleotide 7; **Supplementary Table 1**) and Cy5-GCC TCG CTG CCG TCG CCA-biotin (18-mer, oligonucleotide 12). Cy3-labeled 4R and Cy5-labeled 18-mers were purchased from IDT. 4R 8-oxoG with an amino modifier C7 at the 3′ end was purchased from The Midland Certified Reagent Company and labeled by reaction with Cy3 maleimide (GE Healthcare). Briefly, 3.3 mM Cy3 maleimide was incubated with 40 µM DNA in 100 mM sodium bicarbonate overnight at

room temperature. The excess Cy3 was removed by ethanol precipitation twice. The partial duplex DNA molecules 4R and 4R 8-oxoG were prepared by mixture of a 3′-Cy3 sequence (oligonucleotide 6 or 7) with 18-mer oligonucleotide 12 at a molar ratio of 1:1.5 in 20 mM Tris-HCl, pH 7.5, and 100 mM KCl. The mixtures were incubated at 95 °C for 2 min, then slowly cooled to room temperature at a rate of 2 °C per minute.

**Single-molecule FRET experiments.** smFRET measurements were performed on quartz slides (Finkenbeiner) with glass coverslips, which were coated with polyethylene glycol (PEG). The slides and coverslips were cleaned and treated with methanol, acetone and potassium hydroxide, burned, treated with aminosilane, and coated with a mixture of 97% mPEG (mPEG 5000, Laysan Bio) and 3% biotin-PEG (biotin–PEG 5000, Laysan Bio). Annealed partial-duplex DNA molecules were immobilized on the PEG-passivated surface via biotin-neutravidin interaction. Excess donor molecules were washed away with 10 mM Tris, pH 7.5, and 100 mM KCl with an oxygen-scavenging system (0.5% glucose, 10 mM 6-hydroxy-2,5,7,8-tetramethylchromane-2-carboxylic acid (Trolox), 1 mg/ml glucose oxidase and 4 µg/ml catalase). All measurements were carried out at room temperature. Wide-field prism-type total internal reflection fluorescence (TIRF) microscopy was used with a solid-state 532-nm laser to generate an evanescent field of illumination. Fluorescence signals were separated with a 630-nm dichroic mirror and sent to a charge-coupled device (CCD) camera. Data were recorded with a time resolution of 100 ms as a stream of imaging frames and analyzed with scripts written in Matlab. FRET histograms were generated by using over 6,000 molecules and were fitted to Gaussian distributions with an unrestrained peak center position in Origin 2016. Dwell times were measured on the basis of the time spent by molecules in a low-FRET state. The dwell-time histograms were generated from more than 300 dynamic smFRET traces in at least three separate experiments. The first six transitions were collected from each trace.

**Statistics.** Statistical analyses were performed with R statistical computing language and Prism 6 (GraphPad Software). For **Figures 3b** and **4b,c**, a one-factor ANOVA was used to determine whether the differences between cells expressing a scrambled (scr) shRNA and an shRNA targeting MTH1 mRNA (sh4 and sh5) were significant at a 99% confidence level (Tukey's honest significance test). For **Figures 1**, **3e**, **4e**, **5** and **6**, statistical significance was calculated with two-tailed unpaired Student's *t* tests at a 95% confidence level.

**Data availability. Supplementary information** and uncropped images of gels and blots are available in the online versions of this manuscript. All other data supporting the findings of this study are available from the corresponding author upon reasonable request.

59. Fouquerel, E. *et al.* ARTD1/PARP1 negatively regulates glycolysis by inhibiting hexokinase 1 independent of NAD+ depletion. *Cell Rep.* **8**, 1819–1831 (2014).
60. Latrick, C.M. & Cech, T.R. POT1-TPP1 enhances telomerase processivity by slowing primer dissociation and aiding translocation. *EMBO J* **29**, 924–933 (2010).
61. Pham, H.H. *et al.* Cooperative hybridization of γPNA miniprobes to a repeating sequence motif and application to telomere analysis. *Org. Biomol. Chem.* **12**, 7345–7354 (2014).
62. Ohno, M., Oka, S. & Nakabeppu, Y. Quantitative analysis of oxidized guanine, 8-oxoguanine, in mitochondrial DNA by immunofluorescence method. *Methods Mol. Biol.* **554**, 199–212 (2009).
63. Parikh, D., Fouquerel, E., Murphy, C.T., Wang, H. & Opresko, P.L. Telomeres are partly shielded from ultraviolet-induced damage and proficient for nucleotide excision repair of photoproducts. *Nat. Commun.* **6**, 8214 (2015).
64. Herbert, B.S., Shay, J.W. & Wright, W.E. Analysis of telomeres and telomerase. *Curr. Protoc. Cell Biol.* **20**, 18.16 (2003).

# Corrigendum: Oxidative guanine base damage regulates human telomerase activity

Elise Fouquerel, Justin Lormand, Arindam Bose, Hui-Ting Lee, Grace S Kim, Jianfeng Li, Robert W Sobol, Bret D Freudenthal, Sua Myong & Patricia L Opresko

In the version of this article originally published, the Online Methods section erroneously identified the probe used for immunofluorescence and *in situ* hybridization assays. The error has been corrected for the PDF and HTML versions of this article.